King Saud University

Arabian Journal of Chemistry

www.ksu.edu.sa
www.sciencedirect.com

ORIGINAL ARTICLE

Synthesis and characterization of new polymers derived from 2-methyl-*m*-phenylenediamine as an effective adsorbent for cationic dye removal

Hatice Karaer Yağmur [a,b], İsmet Kaya [a,*]

[a] *Polymer Synthesis and Analysis Laboratory, Department of Chemistry, Çanakkale Onsekiz Mart University, 17020 Çanakkale, Turkey*
[b] *Faculty of Science, Department of Chemistry, Dicle University, 21400 Diyarbakır, Turkey*

Abstract The oxidative polymerizations of 2-methyl-*m*-phenylenediamine were performed to synthesize PMPDIA-A and PMPDIA-B polymers by H_2O_2 (35% aqueous solution) oxidant in acid-catalyzed ethanol and basic aqueous medium. Furthermore, PMPDIA-E polymer of 2-methyl-*m*-phenylenediamine was enzymatically synthesized by HRP (horseradish peroxidase) enzyme and H_2O_2 (35% aqueous solution) in dioxane/0.1 M phosphate tampon solution (pH = 7) mixture. The structures of 2-methyl-*m*-phenylenediamine and polymers were confirmed by FT-IR, NMR and UV–Vis spectrometer measurements. Molecular weight distributions, surface morphologies, thermal and fluorescence properties of polymers were determined from GPC, SEM, TG-DTA, DSC and fluorescence spectra analyses, respectively. CV and UV–Vis analyses were performed to determine the HOMO–LUMO energy levels, electrochemical (E'_g) and optical (E_g) band gaps values of MPDIA, PMPDIA-E, PMPDIA-A and PMPDIA-B. The electrochemical and optical band gaps values of polymers were lower than MPDIA, because of their polyconjugated structures. According to GPC measurements of polymers, the weight average molecular weights were between 5400 and 10400 Da. The fluorescence quantum yield of PMPDIA-E was calculated to be 9.15% in DMSO solution. The adsorption of methylene blue (MB) from aqueous solution on PMPDIA-B was studied. Adsorption isotherms and equilibrium adsorption capacities were determined by the fitting of the experimental data to two well-known isotherm models: Langmuir and Freundlich.
© 2020 Published by Elsevier B.V. on behalf of King Saud University. This is an open access article under the CC BY-NC-ND license (http://creativecommons.org/licenses/by-nc-nd/4.0/).

---

* Corresponding author.
E-mail address: kayaismet@hotmail.com (İ. Kaya).

1. Introduction

In recent years, conjugated polymers (CPs) have attracted much attention of researchers because of their thermal stability, electrochemical and optic properties, and low band gaps (Wen et al., 2019). This can be related to the presence of

π-conjugated structure. This π electrons delocalization decreases the band gap energy value. So, these polymers were used for accumulators, conductive coatings, solar cells, sensors, light-emitting diodes and electro chromic devices.

Phenylenediamines and derivates have been used to synthesize new conjugated polymers (Zoromba and Al-Hossainy, 2020; Sestrem et al., 2010). The aniline is chemically polymerized to synthesize polyaniline. Polyaniline is preferred polymer due to its electrical conductivity. Among the derivatives of aniline, phenylenediamines are the most promising compounds (Blaha et al., 2018). The aromatic diamines such as poly(*m*-phenyldiamine), poly(*o*-phenyldiamine) and poly(*p*-phenyldiamine) can be synthesized by oxidative polymerization reactions using air, NaOCl, H_2O_2 which are known oxidants (Fathy et al., 2020). These polymers are usually synthesized by oxidative polymerization reactions using air, NaOCl, H_2O_2 which are known oxidants (Demir et al., 2006). Poly(phenylenediamine)s have been widely applied for biosensors and sensors, electro catalysis and supercapacitors owing to their the high conductivities and electrochromic properties (Jiang et al., 2020).

Enzymatic oxidative polymerization of phenols has been widely studied by many polymer research groups in the last decades. Syntheses of a variety of poly(aromatics) using aniline and phenol derivatives were accomplished enzymatically using oxidoreductase enzymes under mild reaction conditions in good yields (Kumbul et al., 2016). Enzymatic polymerization is important a method for biosensor development and biocatalysts synthesis. Also, this method is a new approach for synthesis of electronic and optic active polymers. This polymerization has some important benefits such as simple setting, high yields and environmental friendly route. Horseradish peroxidase (HRP) is the most widely used biocatalyst for the polymerization of phenols, anilines, their derivates and a series of new poly(aromatic) compounds in the existence of an oxidant such as H_2O_2 (Turac and Sahmetlioglu, 2010). HRP is an oxidoreductase and it has been widely used for the synthesis of phenol and aniline derivates in the existence of an oxidant such as H_2O_2 (Khosravi et al., 2013). The hydrogen peroxide (H_2O_2) is a compound of great interest in industrial (e.g., mining, textile, and food), pharmaceutical, clinical, environmental topics (in the oxidation of organic molecules) (Tang et al., 2006). Therefore, conjugated polymers can also be synthesized by enzymatic polymerization method and used in semiconductor materials production such as ion exchangers and rechargeable batteries (Çetin et al., 2018). So, syntheses of new poly(phenylenediamine) are important in the production of semiconductor materials. The increases of the environmental pollution have dangerous side effects on water, atmosphere, soil etc. and have severely affected human health. Regarding water; dyes, pesticides, drugs and heavy metals are typical wastewater pollutants and has severely affected human health. With growing human population, synthetic dyes are used in many industrial applications such as food, leather, pharmaceutical and textile. Several methods such as extraction, ion exchange, photo degradation, flocculation, chemical oxidation, coagulation and adsorption have been investigated for removal various pollutants from water. Among these methods, adsorption is a simple and effective technique. But, the preparation of new and effective adsorbents is important (Minisy et al., 2020).

Conjugated polymers, particularly for poly(aniline), poly(pyrrole), poly(thiophene) and their derivatives, have been widely applied in wastewater purification owing to their unique properties, such as easy synthesis, porous structure, good electrorheological property, non-toxicity, etc. (Huang et al., 2014). More types of HRP-catalyzed polymers are required for new applications in wastewater purification, such as poly(phenylenediamine), which is a promising type of polymer with a porous structure.

In present study, 2-methyl-*m*-phenylenediamine (MPDIA) was polymerized by HRP enzyme in 0.1 M phosphate tampon solution (P^H = 7)/dioxane mixture with H_2O_2 as oxidant. Also, MPDIA was polymerized via oxidative polymerization in acid-catalyzed organic medium and basic aqueous medium by H_2O_2 as oxidant. The structure confirm and characterizations of MPDIA, PMPDIA-A, PMPDIA-B, PMPDIA-E polymers were made by FT-IR, NMR, UV–Vis, TG-DTA, CV and fluorescence measurements. Also, GPC, DSC and SEM measurements of polymers were made for molecular weight distributions, surface morphologies and glass transition temperatures (T_g), respectively. Kinetic adsorption studies related to PMPDIA-A and PMPDIA-E were carried out, but their adsorption capabilities were not as strong as PMPDIA-B. So PMPDIA-B was used as an adsorbent. The adsorption of the PMPDIA-B was investigated for removal of methylene blue (MB) from aqueous solution. The adsorption data were fitted to kinetics and isotherm models. Adsorption data were analyzed by both Langmuir and Freundlich adsorption isotherms and the results showed that it was better described by the Freundlich model. The sorption kinetics of MB onto PMPDIA-B was described by the pseudo-second-order kinetic model.

2. Experimental

2.1. Materials

Horseradish Peroxidase (HRP) with a specific activity of 259 purpurogallin units/mg solid and absorbance ratio (Rz) of 3.0. was provided from Sigma-Aldrich Chemical Co. (Germany). 2-methyl-*m*-phenylenediamine (2,6-diamino-toluene) (MPDIA), 0.1 M buffer solution (disodium hydrogen phosphate, pH = 7), ethanol, NaOH, HCl (37% aqueous), 1,4-dioxane and hydrogen peroxide (H_2O_2) (35% aqueous solution) were purchased from Merck Chemical Co. Germany. All compounds were used without purified.

2.2. Enzymatic polymerization of MPDIA

PMPDIA-E was synthesized based on the synthetic routes reported in the literature (Kaya and Kolcu, 2018). The 2-methyl-*m*-phenylenediamine (MPDIA, 0.45 g) was dissolved into 30 mL of 1,4-dioxane in a 100 mL beaker. About 6.0 mg of HRP was dissolved into 7.5 mL 0.1 M phosphate buffer (pH = 7) and the solution added to reaction mixture at 25 °C. The enzymatic polymerization was formed with adding 230 μL of H_2O_2 (35% aqueous solution). Then, 2 mL of H_2O_2 (35% aqueous solution) was added to dropwise within two hours to reaction mixture at room temperature and the mixture was stirred for 24 h. Then, the product was filtrated,

washed with plenty of ethanol and water. The product (PMPDIA-E) was dried at 50 °C in a vacuum oven for 24 h. The reaction procedure and binding of radicals was displayed in Scheme 1. The yield of PMPDIA-E was calculated to be 50%. ^{13}C NMR (DMSO $_{d6}$) δ, ppm: 161.93, 158.94, 152.04, 150.78, 136.93, 133.53, 128.15, 125.85, 120.71, 111.93, 102.59, 72.91, 24.48.

2.3. Syntheses of PMPDIA-B and PMPDIA-A via oxidative polymerization

PMPDIA-B and PMPDIA-A were synthesized reported literature (Şenol and Kaya, 2015; Kaya and Şenol, 2014). PMPDIA-A was obtained through the oxidative polymerization of MPDIA by H_2O_2 (35% aqueous solution) as oxidant in ethyl alcohol medium. 2-methyl-*m*-phenylenediamine (MPDIA) (0.45 g, 3.69×10^{-3} mol) was dissolved in 30 mL of ethyl alcohol placed into a 100 mL two-necked round-bottom flask, which was fitted with a thermometer and condenser. Then, 2 mL acetic acid glacial was added to reaction mixture. Moreover, H_2O_2 (35% aqueous solution) solution (about 2 mL) was

added to dropwise over about 30 min by a funnel containing H_2O_2. The reaction mixture was stirred at 60 °C for 24 h. Then, the mixture cooled to room temperature. The product was precipitated with acetone and filtered to remove it from the solvent. Then product (PMPDIA-A) was dried in a vacuum oven at 50 °C 24 h. The reaction procedure is given in Scheme 2. The yield of PMPDIA-A was calculated to be 45%. ^{13}C NMR (DMSO $_{d6}$) δ, ppm: 153.78, 140.97, 139.32, 138.44, 130.91, 126.72, 123.08, 110.03, 104.20, 92.14, 17.21.

For the synthesis of PMPDIA-B, 2-methyl-*m*-phenylenediamine (MPDIA) was performed in an aqueous alkaline medium by H_2O_2 (35% aqueous solution) as an oxidant in the polymerization reaction. The MPDIA (0.45 g, 3.69×10^{-3} mol) was dissolved in 30 mL of 0.4 M NaOH solution placed into a 100 mL two-necked round-bottom flask which was fitted with a thermometer and condenser. While the mixture temperature was at 70 °C, 2 mL of 35% H_2O_2 was added to the mixture at regular intervals. The mixture was refluxed for 24 h. After the reaction was completed, the mixture was neutralized by HCl (0.4 M). The product was filtrated, washed with plenty of ethanol and water for removed
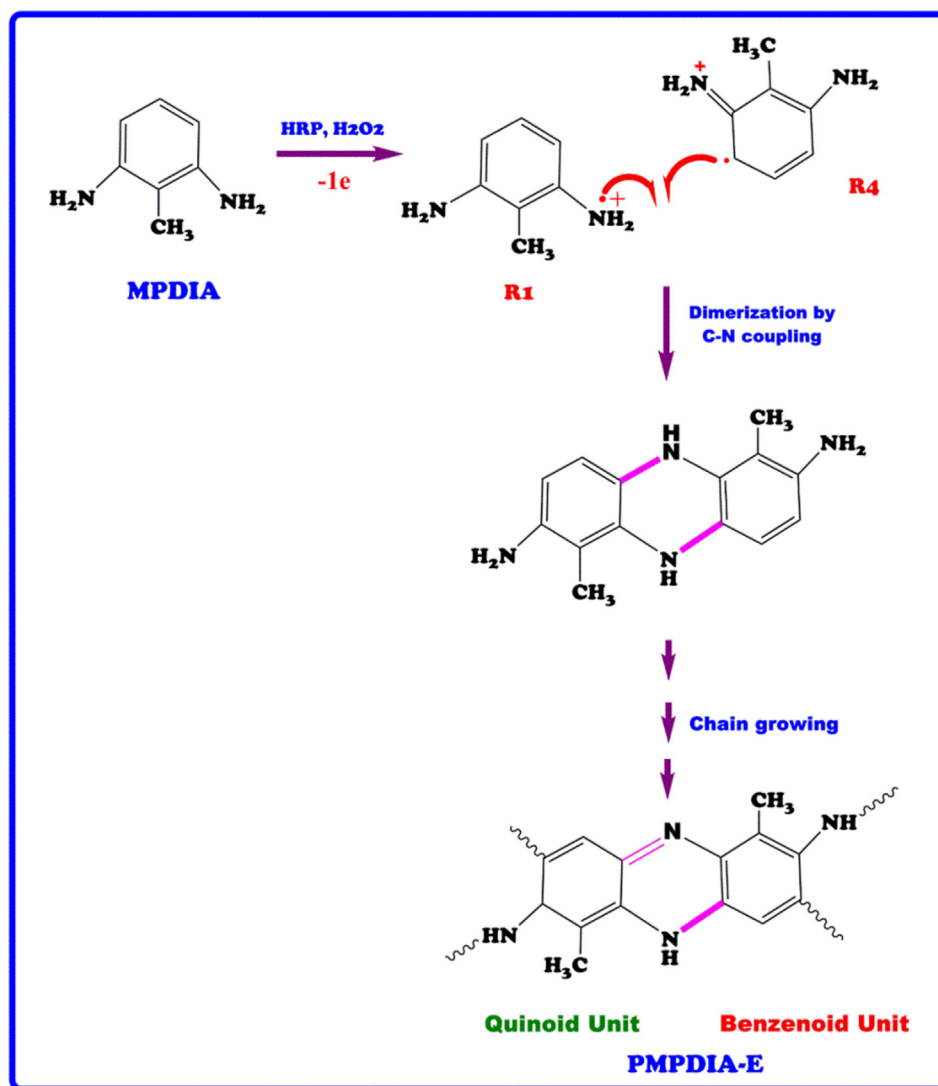
Scheme 1 Synthesis of PMPDIA-E.
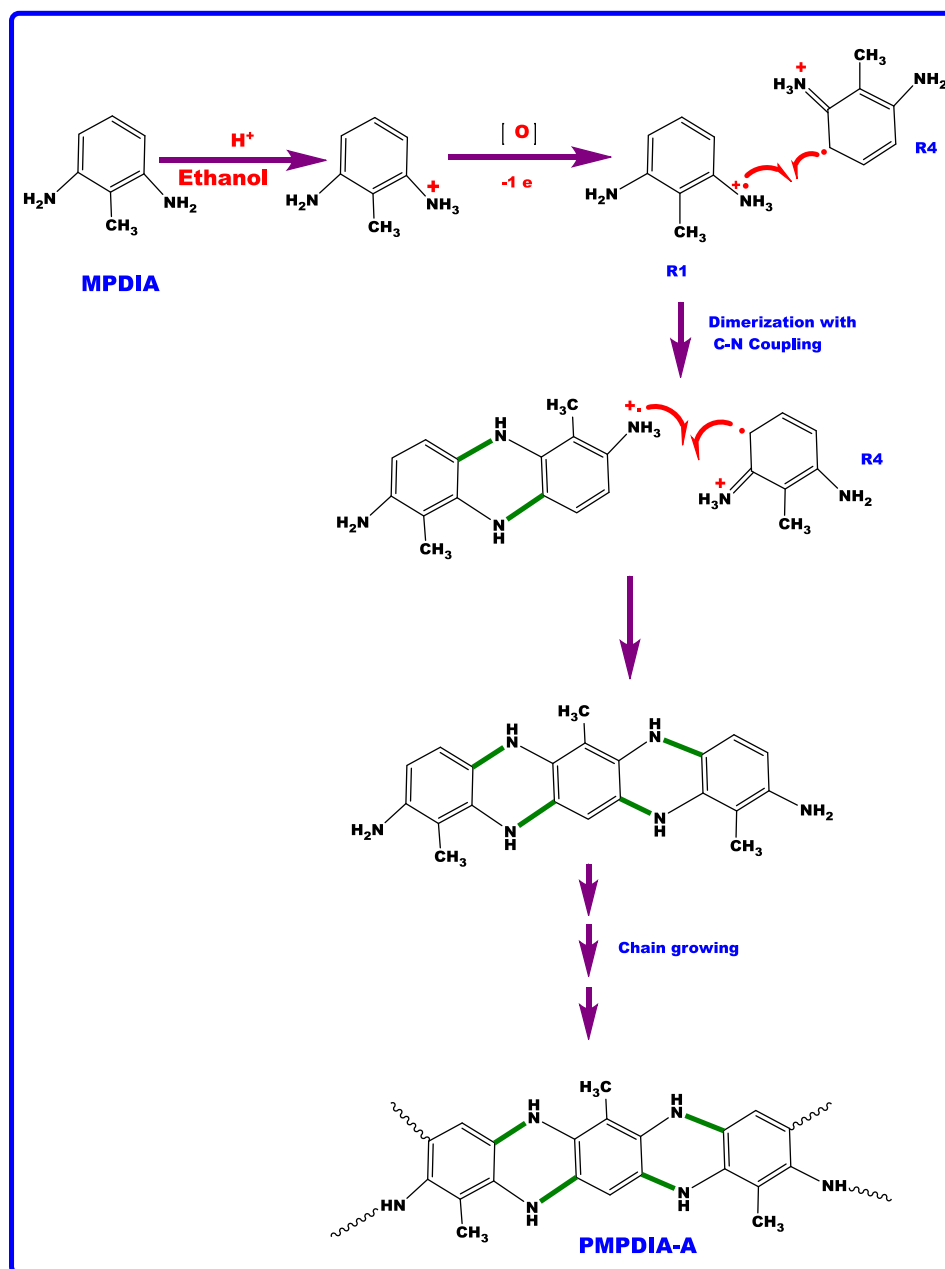
Scheme 2 Synthesis of PMPDIA-A.

salt and unreacted monomer, respectively. After being dried at 50 °C in a vacuum for 24 h, the product (PMPDIA-B) was obtained. Reaction procedure is displayed in Scheme 3. The yield of PMPDIA-B was calculated to be 60%. ^{13}C NMR (DMSO $_{d6}$) δ, ppm: 153.28, 151.70, 139.45, 138.35, 137.40, 129.55, 128.05, 124.15, 118.24, 116.35, 108.66, 105.25, 14.30. The colors of the polymers were brown.

2.4. Characterization

The functional groups of compounds were determined by an infrared spectrophotometer (PerkinElmer Frontier) by attenuated total reflection (ATR) at room temperature (4000–450 cm^{-1}). ^{1}H and ^{13}C NMR spectra were carried out by

Agilent 600 MHz and 150 MHz Premium COMPACT NMR magnet spectrometer at room temperature using DMSO d_6, and tetramethylsilane was used as an internal standard. A Perkin Elmer Diamond Thermal Analysis system (TG-DTA) was used to obtain thermal data of compounds. Perkin Elmer Sapphire Differential Scanning Calorimetry (DSC) was used for determination to the glass transition temperature (T_g) of PMPDIA-E, PMPDIA-B and PMPDIA-A in the range between 25 °C and 450 °C. Both TG-DTA and DSC analyses were performed at a heating rate of 10 °C min^{-1} under N$_2$ atmosphere (200 mL min^{-1}). For thermal analyses measurements were used about 10 mg matters between 20 and 1000 °C at the N$_2$ atmosphere at flow rate 200 mL min^{-1}. The z-average molecular weight (M$_z$), The peak average molec-
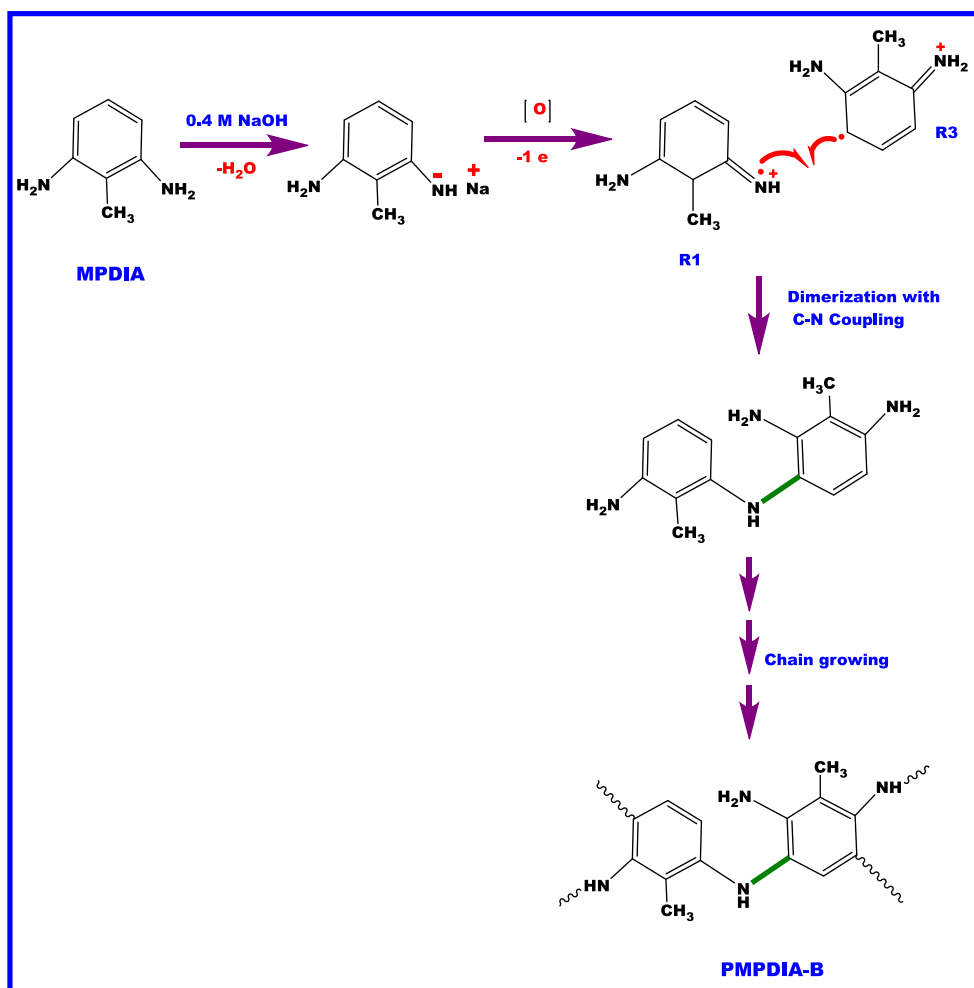
Scheme 3 Synthesis of PMPDIA-B.

ular weight (M_p), the number-average molecular weight (M_n), the average molecular weight (M_w) and the polydispersity index (PDI) of polymers were determined by using Gel Permeation Chromatography-Light Scattering (GPC-LS, Malvern Viscotek GPC Dual 270 max (UK) with a Light Scattering Detector of a medium 8.00 mm x300 mm Dual column and a refractive index detector (RID). SEM (scanning electron microscope) images of the polymers were recorded by SEM JEOL, JSM-7100F model (Japan). Cyclic voltammetry (CV) measurements were performed in 0.1 M tetrabutylammonium hexafluorophosphate (TBAPF6) acetonitrile solution by using a CH 660C Electrochemical Analyzer (CH Instruments, Texas, USA) at a potential scan rate of 20 mV s^{-1}. Fluorescence measurements were performed by a Shimadzu RF-5301PC spectrofluorophotometer. UV–vis analyses were performed by Analytikjena Specord 210 Plus (λ_{max}: 663 nm for MB) spectrophotometer.

2.5. Adsorption experiments

Kinetic experiments were carried out by contacting 100 mL dye solution of the initial concentration of 100 mg L^{-1} with 0.03 g adsorbent (PMPDIA-B) in 100 mL conical flasks at room temperature (25 °C) and natural pH (MB: 7.73). Kinetics of the adsorption was determined by analyzing adsorptive uptake of the dye from aqueous solution at different time intervals.

Adsorption equilibrium studies were carried out by contacting 0.02 g of adsorbent with 100 mL of dyes solution of different initial concentrations (10–100 mg L^{-1}) in 100 mL stopper conical at 25 °C. The mixture was shaken at 500 rpm for 5 h. The amount of adsorbed dye qe (mg g^{-1}) was calculated as follows:

$$qe = (Co - Ce)V/m \qquad (1)$$

Where Co and Ce are the initial and equilibrium concentrations (mg L^{-1}), respectively. V (L) is solution volume and m (g) is the mass of adsorbent.

3. Results and discussion

3.1. Characterization of the polymers

Fig. 1 shows the FT-IR spectra of MPDIA, PMPDIA-A, PMPDIA-B and PMPDIA-E. In MPDIA, two sharp bands observed at 3401 and 3323 cm are related to asymmetrical
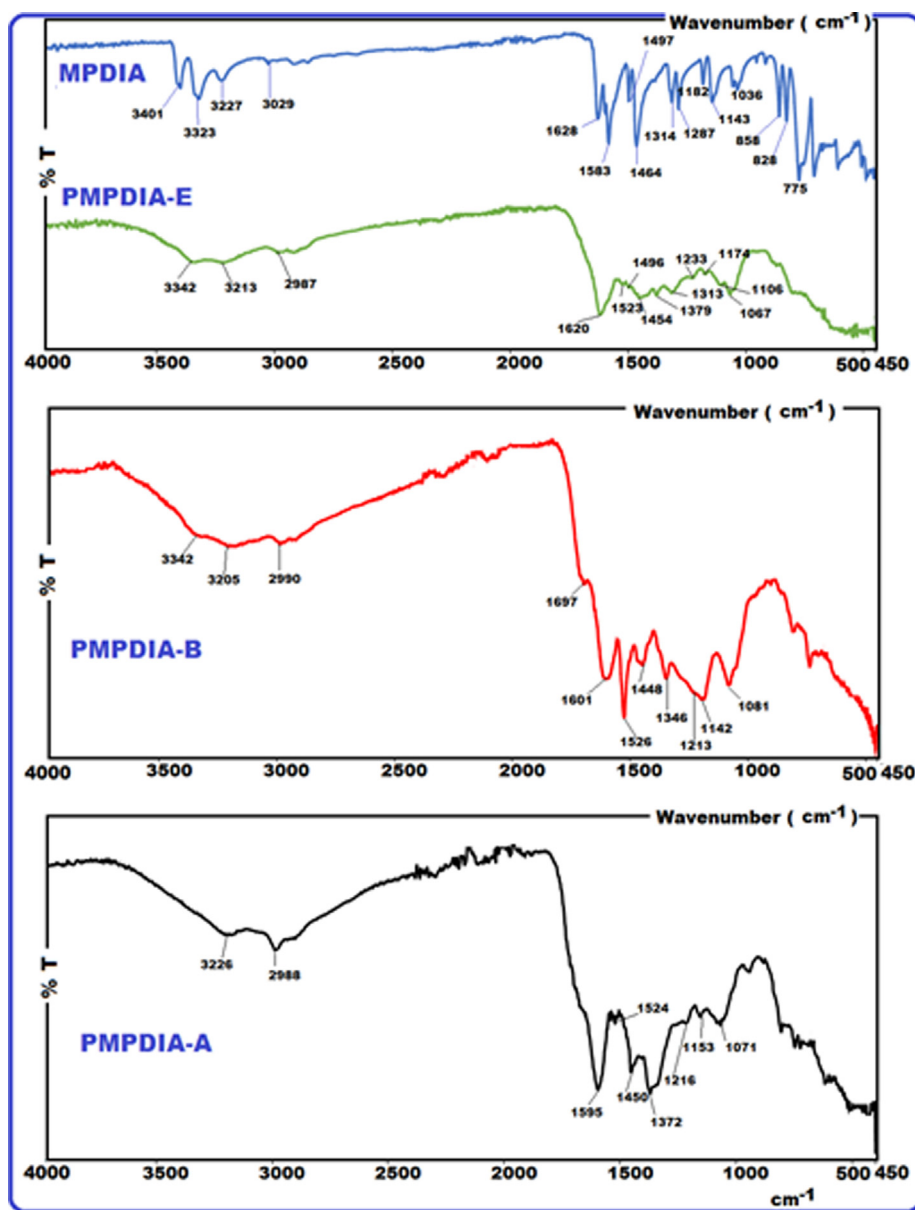
Fig. 1 FT-IR spectra of MPDIA, PMPDIA-E, PMPDIA-B and PMPDIA-A.

(-N-H) and symmetrical (-N-H) stretching modes of NH_2 group. In compounds PMPDIA-A, PMPDIA-E, PMPDIA-A, these bands appear at 3342 and 3205, 3342 and 3213, 3216, respectively, confirming the presence of primary aromatic amine ($-NH_2$) group. The band at 3027 cm^{-1} is $-CH_3$ group in MPDIA. All the polymers shows adsorption band at 2987–2988 cm^{-1} is because of the stretching vibration mode of the -C-H bonds of $-CH_3$ group which is joined to the aromatic ring. 3225–3000 cm^{-1} is the aromatic C-H stretching region, there are no observable bands in FT-IR spectra of polymers, and they merged with $-CH_3$ stretching. –C-H in plane bending appears at the range 1182–1036 cm^{-1} for MPDIA (Gupta et al., 2013). The absorption peaks for MPDIA monomer at 1143, 1054 cm^{-1} are corresponding to in-plane; but 774, 828, 858 cm^{-1} are related to out-of-plane -C-H bending vibration modes (Pramodini et al., 2013).

The bands at 3401 and 3323 cm^{-1} are associated with the primary amine group occur weaker after polymerization because of hydrogen separation from the primary amine group (Şenol and Kaya, 2019). The peaks in the FT-IR spectrum of polymers are broader than those of monomers because of their polyconjugated structures. So, it was observed a decrease in the number of bands (Şenol, 2020). The bands at 3401 and 3323 cm^{-1} are connected to the vibrations of primary amine group of MPDIA were transferred into a secondary amine observed as one broader band at 3226 cm^{-1} for PMPDIA-A characterizing that oxidative polymerization took place on nitrogen atoms of primary amine groups, as observed in Fig. 1. 1142, 1213 cm^{-1} and 1526, 1174, 1233 and 1523 cm^{-1}, 1153, 1216 and 1524 cm^{-1}, are related to the C-C (or C-N) stretching modes for benzenoid ring of PMPDIA-B, PMPDIA-E and PMPDIA-A, respectively (Zoromba and Al-Hossainy, 2020; Minisy et al., 2020;

Pramodini et al., 2013; Olmedo-Martínez et al., 2019; Huang et al., 2001).

The stretching vibration bands of aromatic ring C = C bonding were observed at 1520, 1522 and 1528 cm^{-1} for PMPDIA-B, PMPDIA-A and PMPDIA-E, respectively. The antisymmetric deformation bands of –NH$_2$ or –NH$_2^+$ groups are observed at 1465, 1444, 1447 and 1454 cm^{-1} for MPDIA, PMPDIA-A, PMPDIA-B and PMPDIA-E, respectively. The similar results were determined for these functional groups in obviously studies (Bilici et al., 2010). The above results are in agreement with one other the reported results (Gupta et al., 2013; Pramodini et al., 2013). These results confirm the molecular structure of the synthesized polymers. As stated in the previous studies, amine-based monomers can be polymerized by phenylene (C-C) or (C-N) couplings by nitrogen atom of –NH$_2$ coupling of monomer units with *ortho* or *para* position of the phenylendiamine in terms of –NH$_2$ group (Topal et al., 2017). Since (–NH$_2$) group is *ortho* and *para* directing group in the aromatic ring, the syntheses of polymers are expected to occur via the coupling of carbon radicals abbreviated as R1, R2, R3 and R4. Scheme 4 shows the possible four radicalic forms of MPDIA and different coupling forms for the synthesis of polymers. Therefore, polymers were ascribed to comprise the *ortho–ortho*, *ortho–para* and amine-*ortho* connected phenyl repeat units.

MPDIA was polymerized acidic and basic media with H$_2$O$_2$. Moreover, MPDIA monomer was then enzymatically polymerized in the existence of HRP enzyme with H$_2$O$_2$, resulting in the formation of radicals, which were then linked via C-C, N-N and C-N-C couplings. The most probable route for the polymerization method was through the coupling of R1 and R4 (or R3) concurrent resulting in C-NH-C bond formations (Scheme 4) (Kolcu, 2019).

Fig. 2 (A) and (B) show the ^{13}C NMR and ^{1}H NMR spectra of the MPDIA respectively. In the ^{1}H NMR (Fig. 2 A) spectra of MPDIA, four signals observing at 6.59 (triplet), 5.96 (doublet), 4.45 (singlet) and 1.82 (singlet) ppm were related to aromatic -Ha, -Hb, –NH$_2$, and –CH$_3$ protons, respectively. In the ^{13}C NMR (Fig. 2 B) spectra of MPDIA, five signals are seen at 146.96, 125.47, 105.43, 104.69 and 11.20 ppm and these values were related to C5, C4, C3, C2 and C1 carbon atoms, respectively.
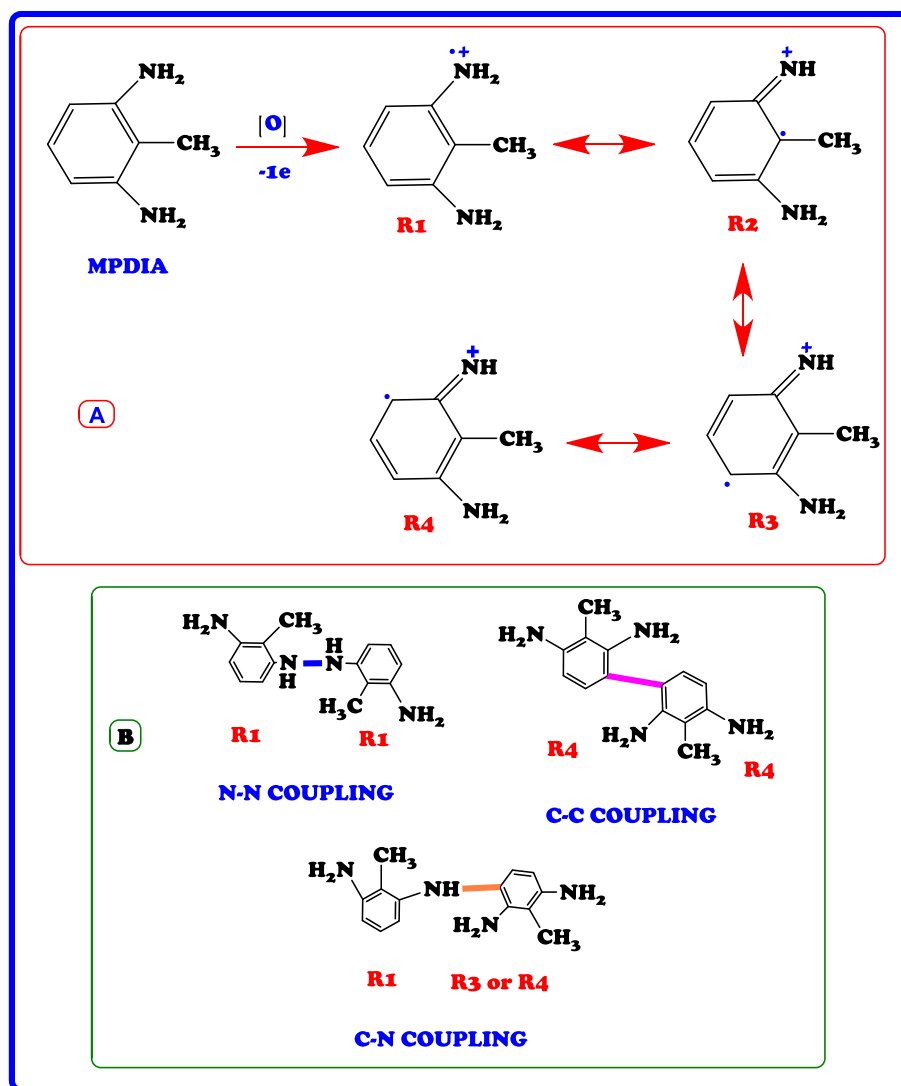
Scheme 4 Possible resonance structures MPDIA (A) and different coupling states of radicals of MPDIA (B).
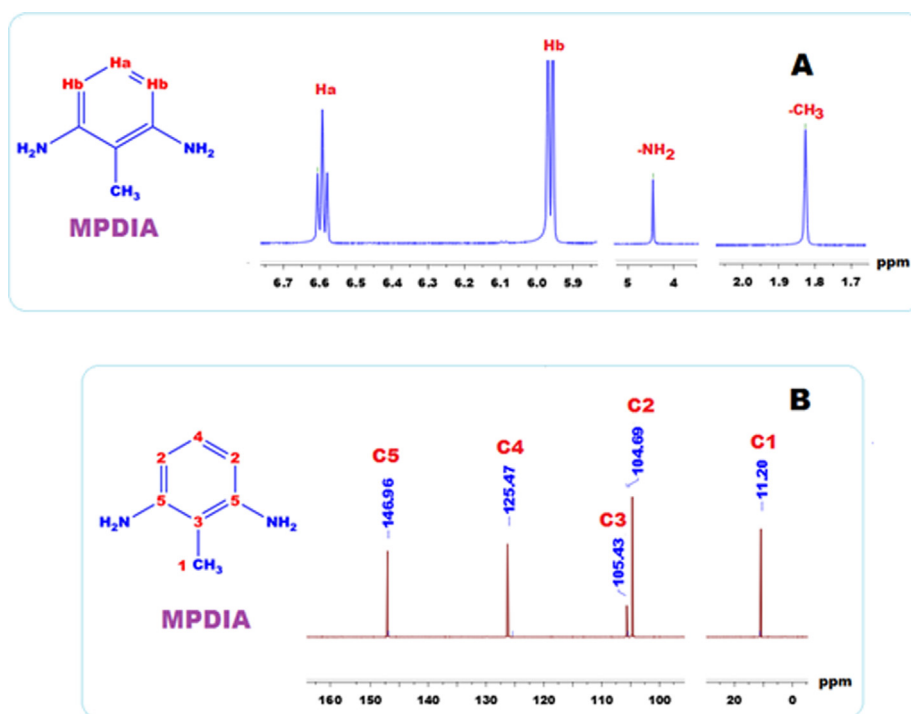
Fig. 2 ^{1}H NMR (A) and ^{13}C NMR (B) spectra of MPDIA in DMSO d_6.

Fig. 3 shows the ^{1}H NMR spectra of PMPDIA-E, PMPDIA-B and PMPDIA-A. The peaks appeared at 9.90, 7.39 and 2.08 ppm were assigned to –NH, aromatic -Ha and –CH$_3$ protons of PMPDIA-E. The signals of –NH, and –NH$_2$, aromatic -Ha, -Hb, –Hc and –CH$_3$ protons of PMPDIA-B were observed at 9.14, 5.86 ppm and 5.14 ppm, 7.20, 7.00, 6.90 ppm and 2.04 ppm, respectively. The peaks at 10.00, 7.46 and 1.29 ppm were related to –NH, aromatic -Ha and –CH$_3$ protons of PMPDIA-A. The ^{1}H NMR spectra of polymers show broad signals for aromatic protons which confirm the participation of aromatic ring in polymerization (Kaya et al., 2017). According to the ^{13}C NMR result of MPDIA, the signal of the carbon atom to which the nitrogen atom is attached was observed at 146.96 ppm. On the other hand, the signals of these carbon atoms in PMPDIA-E PMPDIA-A PMPDIA-B were observed at 161.93, 153.78 and 153.28 ppm, respectively. The shifting of these values to the lower field shows that ringing and conjugation occurred in the structure of polymers. The shifting to the lower field of this carbon atom of the enzymatic polymer was demonstrated to be formation of -C = N- group into of ring in the structure. Also, new peaks were observed due to polymerization at the ^{13}C NMR spectra of PMPDIA-E PMPDIA-A PMPDIA-B as different from the monomer.

The M$_w$, M$_n$, PDI, M$_z$ and M$_p$ values of polymers were defined by GPC analysis and displayed in Table 1. GPC curves of obtained polymers were displayed in Fig. 4. Although the high molecular weight polymer can be synthesized by chemical oxidative polymerization (Khosravi et al., 2013; Bilici et al., 2010), the enzymatic polymerization leads to the formation of an oligomer. According to Table 1, the average molecular weight values were as follows PMPDIA-B > PMPDIA-E > PMPDIA-A. PMPDIA-B has higher molecular weight than

PDIABA-E and PMPDIA-A owing to more active radical centers (Kaya and Kolcu, 2018; Temizkan and Kaya, 2020). The Mw values of PMPDIA-A, PMPDIA-B and PMPDIA-E were found to be 5400, 10,400 and 10000 Da, respectively. It is seen that Fig. 4, two peaks were observed at chromatogram of PMPDIA-A. These values of PMPDIA-A were calculated according to main peak in the chromatogram.

3.2. Thermal analysis

The TG and DTG curves of compounds were given in Fig. 5. The TG and DTG data of the MPDIA, PMPDIA-A, PMPDIA-B and PMPDIA-E were given in Table 2. According to DTA analysis of MPDIA, endothermic peaks were observed at 106 and 206 °C. MPDIA was degraded one step. While PMPDIA-E and PMPDIA-B were degraded at the two steps, PMPDIA-A was degraded at the three steps. According to the TG curves of PMPDIA-E, PMPDIA-A and PMPDIA-B, the moisture or organic solvents were removed between 50 and 105 °C. These values of PMPDIA-E, PMPDIA-A and PMPDIA-B were found to be 5.20, 7.35 and 3.0%, respectively. The starting degradation temperatures (T$_{on}$) were 176, 135, 124 and 137 °C for MPDIA, PMPDIA-E, PMPDIA-A and PMPDIA-B, respectively. The first step and second step of PMPDIA-E were observed between 105 and 706 °C and 706–1000 °C as 48.02% and 19.31% mass losses, respectively.

The temperatures in related to 20% (T$_{20}$) weight loss were determined as 179, 264, 210 and 275 °C for MPDIA, PMPDIA-E, PMPDIA-A and PMPDIA-B, respectively, and the temperatures corresponding to 50% (T$_{50}$) weight loss were 199, 766, 560 and 710 °C for MPDIA, PMPDIA-E, PMPDIA-A and PMPDIA-B, respectively. The residual amounts of PMPDIA-E, PMPDIA-A and PMPDIA-B were determined
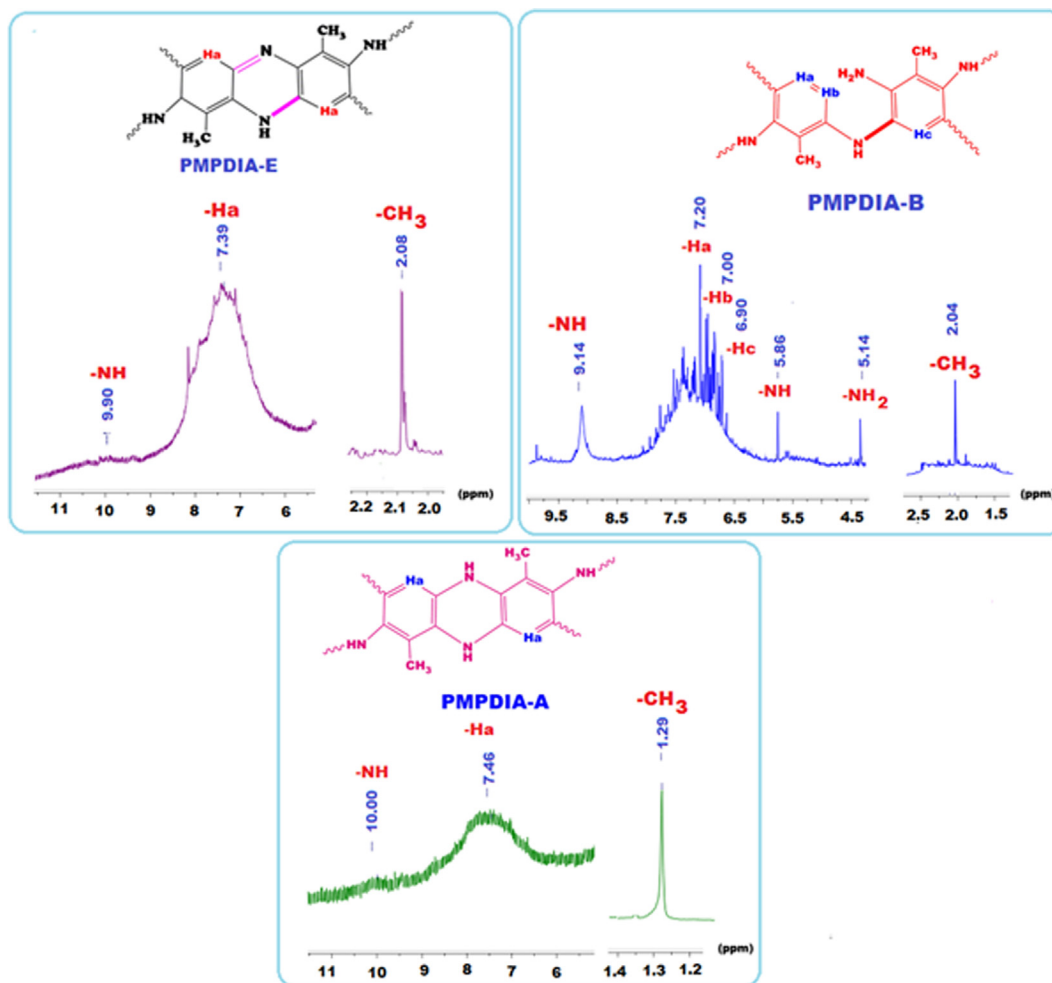
Fig. 3 ^{1}H NMR spectra of PMPDIA-E, PMPDIA-B and PMPDIA-A in DMSO d_6.

Table 1 GPC results of polymers.

Polymer	Mn	Mw	PDI	Mz	Mp
PMPDIA-E	7100	10,000	1.408	11,400	7350
PMPDIA-A	4650	5400	1.161	6500	4450
PMPDIA-B	8250	10,400	1.261	13,200	5650

to be 32.77%, 18.76% and 37%, respectively, nitrogen atmosphere at 1000 °C. It is seen in Table 2, the PMPDIA-E was more thermally stable than the PMPDIA-A and PMPDIA-B. SEM images of PMPDIA-E also was confirmed this result. Because PMPDIA-E was at a spherical structure. The glass transition temperatures (T_g) of PMPDIA-E, PMPDIA-A and PMPDIA-B were found to be 114, 101 and 96 °C, respectively. The ΔCp values which calculation from the glass transition temperatures of PMPDIA-E, PMPDIA-A and PMPDIA-B were found to be 0.236 J g^{-1}°C^{-1}, 0.382 J g^{-1}°C^{-1} and 0.194 J g^{-1} °C^{-1}, respectively.

3.3. Surface morphologies of polymers

SEM images of PMPDIA-B, PMPDIA-A and PMPDIA-E were shown in Fig. 6. It is seen that Fig. 6, although H$_2$O$_2$ was used as oxidant in all polymerizations, the appearance of each polymer was different because the reaction environments were different. While the PMPDIA-E formed in enzymatic polymerization is spherical, the PMPDIA-B formed in oxidative polymerization (alkaline) has a spongy structure. PMPDIA-A formed in the acid-catalyzed ethanol medium was both a spongy and partially spherical surface.
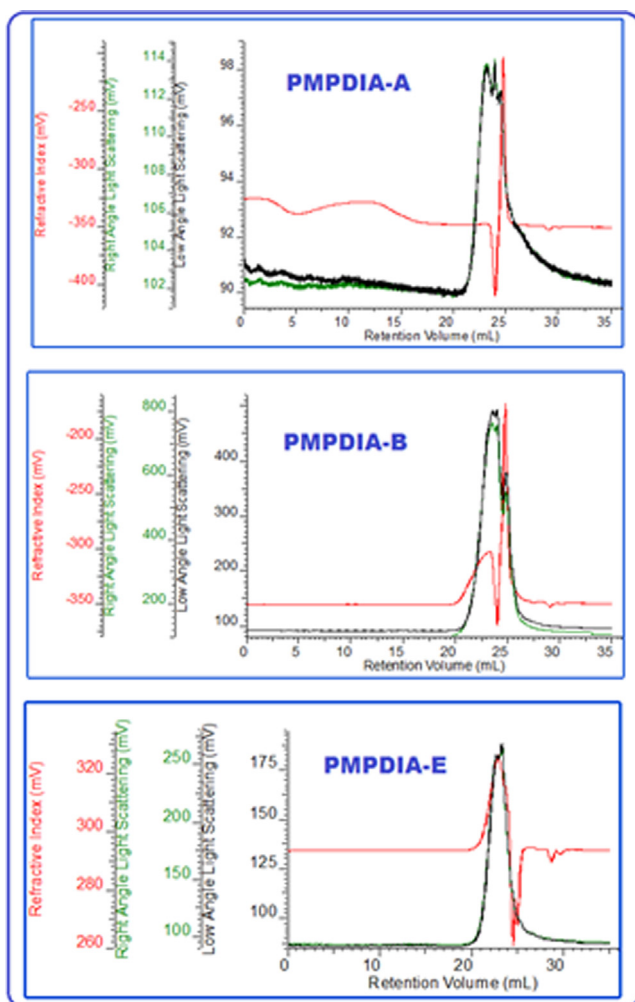
Fig. 4 GPC chromatograms of PMPDIA-A, PMPDIA-B and PMPDIA-E.

3.4. Fluorescence properties

Fluorescence features of samples were performed using DMSO solutions. The MPDIA and PMPDIA-B have demonstrated low fluorescence emission intensity in DMSO solutions. Fig. 7 (A) shows monomer (0.05 mg mL^{-1}) and polymers (0.05 mg mL^{-1}) fluorescence intensity. Fig. 7 (B) shows emission spectra of the synthesized PMPDIA-E were defined in different concentration such as 0.05, 0.025, 0.0125 and 0.0625 mg mL^{-1} in DMSO solution. According to 0.0625 mg mL^{-1} concentration of PMPDIA-E, the highest fluorescence intensity was seen when stimulated with 350 nm. When excited at 350 nm, blue emissions were seen at 0.05, 0.025, 0.0125 and 0.0625 mg mL^{-1} in DMSO solutions for PMPDIA-E. Fig. 7 (C) shows the visible colors of PMPDIA-E under UV light and sunlight, respectively. The brown solution of PMPDIA-E turned into turquoise under UV-lamp. The fluorescence quantum yield of PMPDIA-E was found based on reported literature (Temizkan and Kaya, 2020) and was defined as 9.15%, when excited at 350 (for slit 5 nm) in DMSO solution.
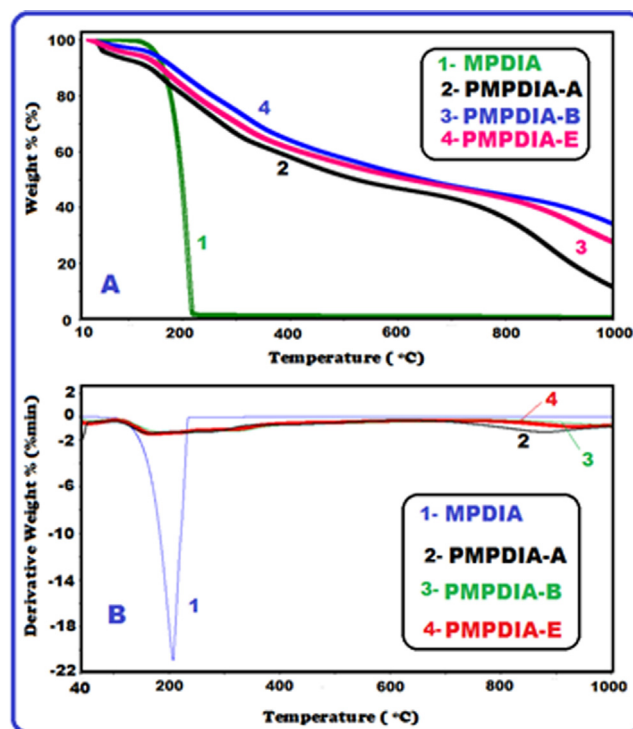
Fig. 5 TG (A) and DTG (B) curves of MPDIA, PMPDIA-A, PMPDIA-B and PMPDIA-E.

3.5. Electrochemical and optical properties

The UV–Vis spectra of MPDIA, PMPDIA-A, PMPDIA-B and PMPDIA-E were performed in DMSO, at room temperature and displayed in Fig. 8. The observed peak in 335 nm in Fig. 8 (for PMPDIA-E) is related to $\pi \rightarrow \pi^*$ transition of the quinoide rings. It is assigned to the extent of conjugation between the phenyl rings along the polymer chain (Pramodini et al., 2013; Temizkan and Kaya, 2020). Furthermore, the bathochromic shift and the tail of the transitions into the visible region (400–700 nm) could be attributed to the formation of a long poly(aromatic) conjugated system during polymerization (Turac and Sahmetlioglu, 2010).

The band at 265 nm is related to the $\pi \rightarrow \pi^*$ transition in benzenoid rings neighboring with amine (Blaha et al., 2018). According to the UV–visible spectra (Fig. 8), if absorption maximum is below 265 nm, this displays benzenoid rings connected to the amine nitrogen. The absorption bands in below of 300 nm is generally related to the $\pi \rightarrow \pi^*$ electronic transitions of the benzene or benzenoid rings (Turac and Sahmetlioglu, 2010; Blaha et al., 2018; Pramodini et al., 2013). The $\pi \rightarrow \pi^*$ electronic transitions of MPDIA, PMPDIA-A and PMPDIA-B were observed at 297, 281 and 292 nm, respectively. The optical band gaps (E_g) of polymers were determined the literature (Kamacı and Kaya, 2016) by following equation.

$$E_g = 1242/\lambda_{onset} \qquad (2)$$

The values E_g were given in Table 3. The λ_{onset} is the starting wavelength for the electronic transition which can be defined using absorption edges of UV–vis spectra (Kamacı

Table 2 Thermal data of compounds.

Compounds	TGA (°C)				
	[a]T_{onset}	[b]T_{20}	[c]T_{50}	[d]%Char	[e]T_{max}
MPDIA	176	179	199	0.59	206
PMPDIA-E	135	264	766	32.77	135,174
PMPDIA-A	124	210	560	18.76	233, 411, 878
PMPDIA-B	137	275	710	37.00	206, 317, 656

[a]T_{onset}, the onset temperature.
[b]T_{20}, temperature corresponding to 20 wt% weight loss.
[c]T_{50}, temperature corresponding to 50 wt% weight loss.
[d] %Char, % Carbine residue at (1000 °C).
[e]T_{max}, temperature of the maxima of the peak.
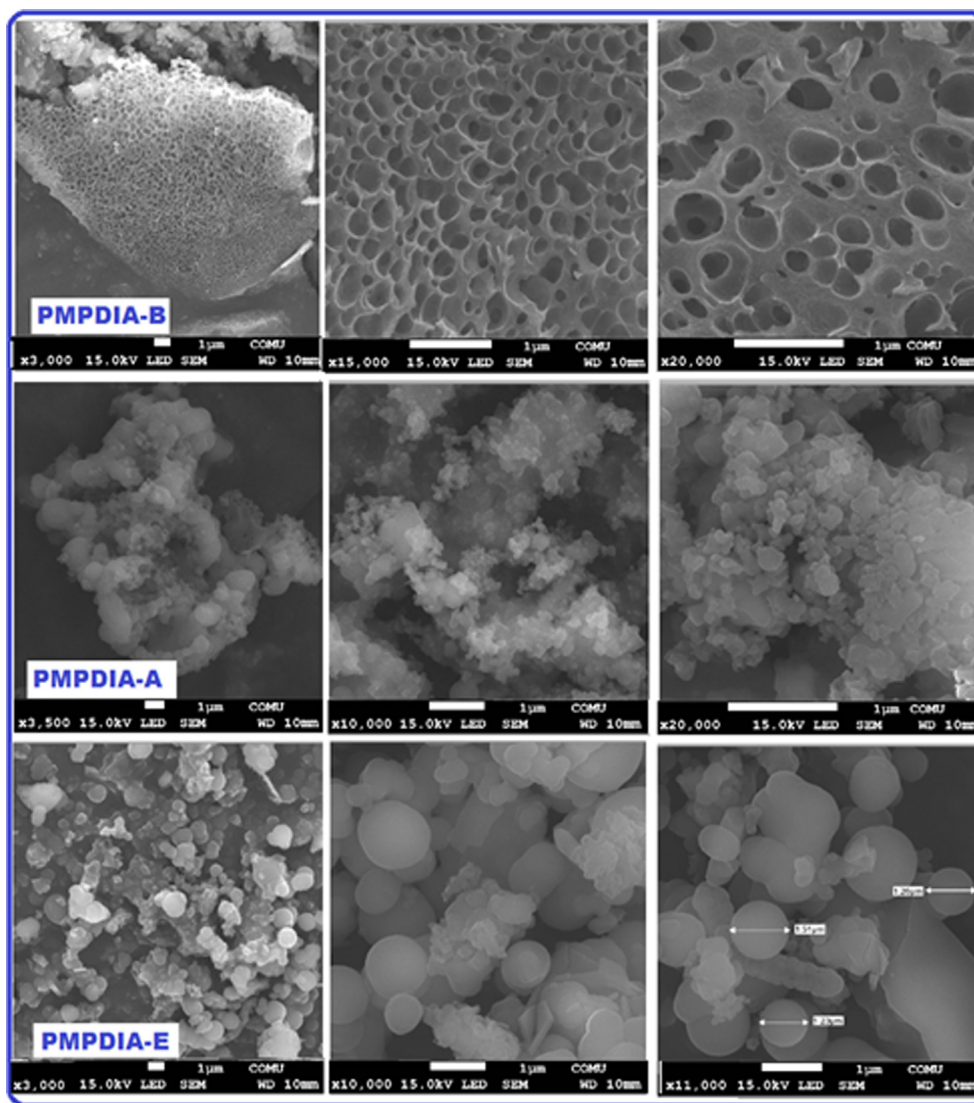
Fig. 6 SEM images of PMPDIA-B, PMPDIA-A and PMPDIA-E.

and Kaya, 2016). The λ_{onset} values of MPDIA, PMPDIA-A, PMPDIA-B and PMPDIA-E as displayed in Table 3 were defined as 321, 452, 553 and 561 nm, and the E_g values were found as 3.87, 2.75, 2.24 and 2.21 eV in DMSO, respectively.

According to results, the E_g values of polymers were lower than MPDIA monomer. This situation is due to the creation of traps in the polymer electrolyte and the formation of free radicals (Gao et al., 2019).
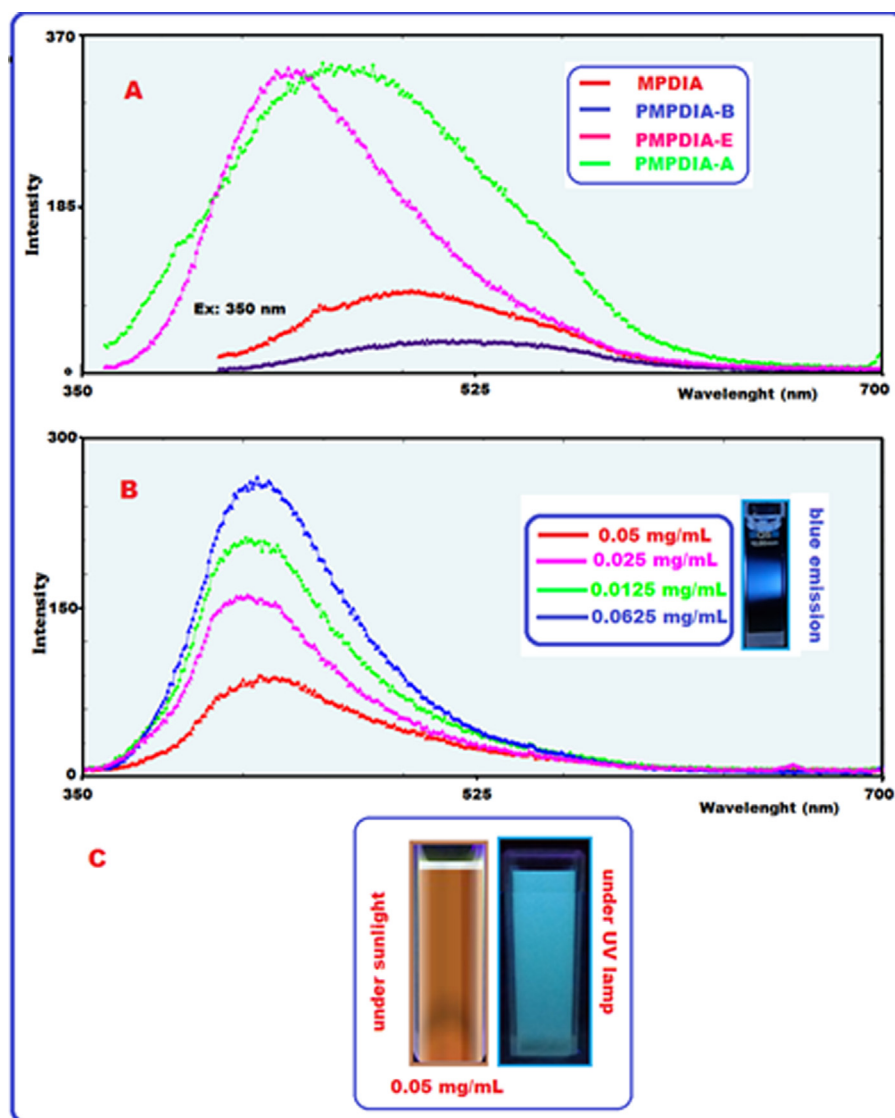
Fig. 7 PL spectra of MPDIA, PMPDIA-A, PMPDIA-B, PMPDIA-E (A), PL intensity of PMPDIA-E with 0.05, 0.025, 0.0125 and 0.0625 mg mL^{-1} (at slit 5 nm) (B) and PMPDIA-E under UV light and sun light in DMSO (C).
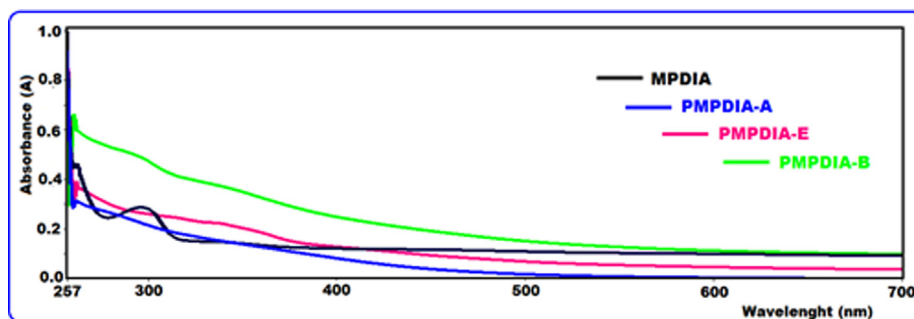
Fig. 8 The UV–Vis spectra of monomer and polymers.

Fig. 9 shows the curves of CV. The values of electrochemical band gaps (E'_g) were obtained by using the oxidation onset (E_{ox}) and reduction onset (E_{red}) values by cyclic voltammetry (CV) measurements, as shown Fig. 9 for PMPDIA-A, PMPDIA-B and PMPDIA-E where E_{ox} is the oxidation peak potential and E_{red} is the reduction peak potential. The values of HOMO and LUMO were determined by using the following equations (Şenol et al., 2019):

Table 3 Optical electronic structure parameters of PMPDIA-A, PMPDIA-B and PMPDIA-E.

Compounds	λ_{max} (nm)	λ_{onset} (nm)	$^{a}E_g^{a}$ (eV)	HOMO[b] (eV)	LUMO[c] (eV)	$E'_g{}^{d}$ (eV)
MPDIA	297	321	3.87	5.70	2.58	3.12
PMPDIA-A	281	490	2.53	5.87	2.95	2.92
PMPDIA-B	292	502	2.47	5.98	3.11	2.87
PMPDIA-E	335	582	2.13	5.72	3.30	2.42

[a]Optical band gap. [b]Highest occupied molecular orbital. [c]Lowest unoccupied molecular orbital. [d]Electrochemical band gap.
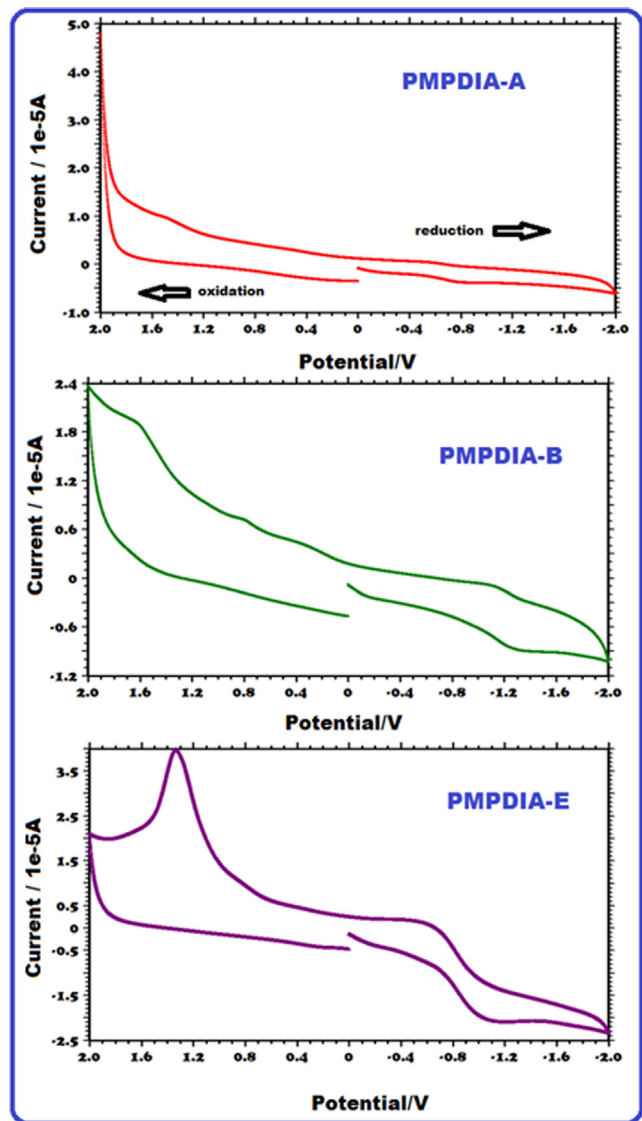
Fig. 9 CV cycles of PMPDIA-A, PMPDIA-B and PMPDIA-E.

$$E'_g = E_{LUMO} - E_{HOMO} \tag{3}$$

$$E_{HOMO} = -(4.39 + E_{ox}) \tag{4}$$

$$E_{LUMO} = -(4.39 + E_{red}) \tag{5}$$

To understand the electronic structure of conjugated polymers it is essential to determine the highest occupied molecular orbital (HOMO) and the lowest unoccupied molecular orbital (LUMO) (Li et al., 2016).

The E'_g values of MPDIA, PMPDIA-A, PMPDIA-B and PMPDIA-E were determined as 3.12, 2.92, 2.87 and 2.42, respectively. Based on Table 3, the values of E'_g of PMPDIA-A, PMPDIA-B and PMPDIA-E were lower than MPDIA monomer. The values of the electrochemical band gap of PMPDIA-A, PMPDIA-B and PMPDIA-E are lower due to the polyconjugated structure (Yuvaraja et al., 2020).

3.6. Adsorption studies

The kinetic study was performed at 298 K. The adsorption kinetics describes the rate of adsorbate molecules uptake on the adsorbents (Minisy et al., 2020). Kinetical data corresponding to the effect of contact time were analyzed by using the pseudo-first-order (PFO, Lagergren) Eq. (6), the pseudo-second-order (PSO, Ho-Mckay) Eq. (7) and intraparticle diffusion models (Eq. (8)). Fig. 10 shows non-linear kinetics of MB adsorbed on PMPDIA-B at 298 K (Fig. 10 (A), the effect of the contact time) and the curves of linear kinetic models, such as pseudo first-order model (Lagergren) (Fig. 10 (B), pseudo second-order model (Ho-Mckay) (Fig. 10 (C) and intraparticle diffusion model (Fig. 10 (D).

$$\log(q_e - q_t) = \log q_e - k_1 t/2.303 \tag{6}$$

$$t/q_t = 1/k_2 q_{e2} + t/q_t \tag{7}$$

$$q_t = k_{id} t^{1/2} + C \tag{8}$$

where qe and qt are the amount of sorbed in equilibrium and at time t, respectively, $k_1(min^{-1})$, k_2 (g mg^{-1} min^{-1}) and k_{id} (mg g^{-1} min$^{-1/2}$) are the equilibrium rate constant of PFO, PSO and the intraparticle diffusion rate constant, respectively (Han, 2008; Kant, 2012). Furthermore, the average relative error (ARE) can be calculated to define the most suitable kinetic model. The equation is given as follows (Tseng et al., 2010):

$$ARE = \frac{100}{n} \sum_{n=1}^{n} \left(\frac{qe, \exp - qe, cal}{qe, \exp} \right) \tag{9}$$

where $q_{e,cal.}$ and $q_{e,exp.}$ (mg g^{-1}) are the model predicted and experimental adsorption capacity of at time t, respectively, and n is the number of observations. Low ARE values show the accurate fitting of the model. The values of ARE, kinetic data and the correlation coefficient R^2 were given in Table 4. Based on Table 4, the best fitting of the experimental adsorption data to the pseudo-second order could be confirmed from the $q_{e,calc.}$ which was close to $q_{e,exp.}$ and also calculated coefficients of determination (R^2) which was grater for pseudo-second order model. Low ARE values show the suitability of
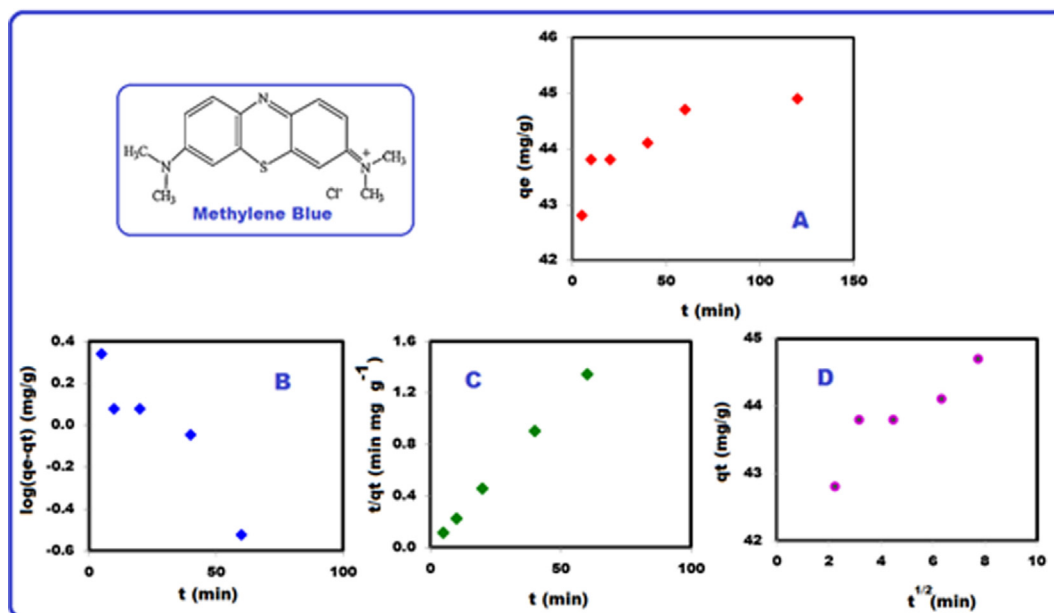
Fig. 10 Adsorption kinetic of MB on PMPDIA-B at 298 K (A), fitting of Lagergren (PFO) (B), Ho-Mckay (PSO) (C) and intraparticle diffusion model (D).

Table 4 Kinetic parameters.

Kinetic models	Parameters	R^2	ARE
Pseudo first-order (PFO, Lagergren)	$q_{e,cal.} = 2.19$ mg g^{-1} $q_{e,exp.} = 45.0$ mg g^{-1} $k_1 = 0.03017$ min^{-1}	0.885	50.68
Pseudo second-order (PSO, Ho-Mckay)	$q_{e,cal.} = 44.84$ mg g^{-1} $q_{e,exp.} = 45.0$ mg g^{-1} $k_2 = 0.06721$ g/(mg min)	0.9999	2.79
intraparticle diffusion model	k_{id}:0.2787 mg g^{-1} min$^{-1/2}$	0.8358	–

the model (Tseng et al., 2010). According to the results, the pseudo-second order (PSO) model better fits to the kinetic data than pseudo-first order model (PFO).

The adsorption isotherm was used to describe the equilibrium distribution of dye molecules at the solid–liquid phases. The most common adsorption isotherm models: Temkin, Freundlich and Langmuir were used to investigate the sorbate-sorbent interactions.

The Langmuir model is monolayer adsorption isotherm. According to Langmuir isotherm, the adsorbent surface is homogeneous, energetically uniform. According to Freundlich isotherm, the adsorbent surface is heterogenous. Freundlich isotherm is convenient adsorption at high concentrations and not convenient for the low concentration range (Jawad et al., 2019). Tempkin isotherm suggested that due to the sorbate- sorbent interactions, the energy of the adsorption of the molecules will decrease linearly with coverage (Ghani et al., 2013). The equilibrium data were applied to Langmuir (Eq. (10)), Freundlich (Eq. (11)) and Temkin (Eq. (12)) isotherm models.

$$C_e/q_e = 1/KaQ_{max} + Ce/Q_{max} \qquad (10)$$

$$logqe = logK_f + (1/n)logCe \qquad (11)$$

$$q_e = blnK_T + blnC_e \qquad (12)$$

where Q_{max} (mg g^{-1}) is the maximum adsorption capacity of dye adsorbed per unit mass of adsorbent at equilibrium (mg g^{-1}) and Ka (L mg^{-1}) is the Langmuir isotherm constant. k is the Freundlich isotherm constant which corresponding to the adsorption capacity of the adsorbent and n is the adsorption intensity. K_T is the Temkin isotherm constant which corresponds to the maximum binding energy and b is a Temkin constant corresponding to the heat of adsorption (J mol^{-1}) (Yapa et al., 2017). Table 5 shows a summary of some of the recent application of some adsorbents for the removal of some dyes from wastewater (Nandi and Purkait, 2009; Doğan et al., 2006; Bulut and Karaer, 2015; Iqbal and Ashiq, 2007; Mahdavinia et al., 2014; Kaya and Yağmur, 2020).

The root mean squared error (RMSE), sum of the squares of the error (SSE) and standard deviation (SD) can be calculated to determine the most suitable isotherm model (Abbas et al., 2020; Fajri et al., 2018) as shown in Table 6. The values of RMSE (Eq. (13)), SSE (Eq. (14)) and SD (Eq. (15)) can be calculated by the following equations:

Table 5 Comparison of maximum monolayer capacity for MB on the other different adsorbents.

Adsorbent	Qm (mg g^{-1})	References
Poly(2-methyl-*m*-phenylenediamine)	1428.57	This work
Fly ash	13.42	39
Rice husk	40.58	40
Activated charcoal	25.25	41
Commercial activated carbon	22.3	42
Chitosan-clay composite	142	43
poly(3,5-diaminobenzoic acid)	53.19	44

$$RMSE = \sqrt{\frac{1}{n-1}\sum_{n=1}^{n}(q\exp. - q cal.)^2} \quad (13)$$

$$SSE = \sum_{n=1}^{n}(q cal. - q\exp.)^2 \quad (14)$$

$$SD = \sqrt{\frac{1}{n}\sum_{n=1}^{n}(q\exp. - q cal.)^2} \quad (15)$$

Where n is the number of observations. Fig. 11 (A), (B) and (C) show the Langmuir, Freundlich and Temkin isotherm models for the adsorption of MB at 298 K. The values of errors (RMSE, SSE and SD), adsorption isotherm parameters and correlation coefficients (R^2) were shown in Table 6. Based on Table 6, the values of RMSE, SSE and SD calculated from Freundlich isotherm model were lower than Langmuir isotherm model and Temkin isotherm model. Low SD, RMSE and SSE values indicate the suitability of the isotherm model (Abbas et al., 2020; Fajri et al., 2018). The Freundlich isotherm describes the multilayer adsorption of sorbate on a heterogeneous surface of the sorbent. The heterogeneity factor (n) shows if the adsorption process is physical (n > 1), chemical (n < 1) and linear (n = 1) (Ghani et al., 2013; Fungaro et al., 2009).

The adsorption mechanism of MB dye on the PMPDIA-B surface was happened by different interactions. The adsorption mechanism also includes H-bonding interactions that can be occurred between H and N atoms available on the surface of PMPDIA-B, and N atom in the MB dye structure. Finally, n-π interaction comes from the delocalization of the lone pair electron of N atoms into the π orbital of the dye aromatic ring (Jawad and Abdulhameed, 2020).
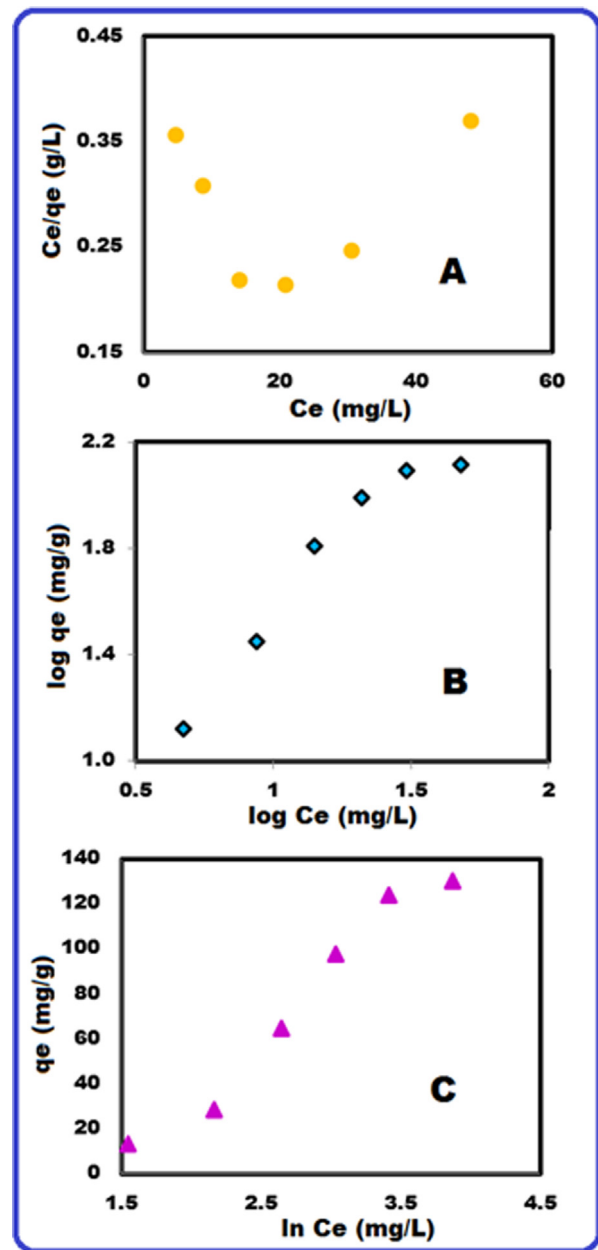
Fig. 11 Langmuir (A), Freundlich (B) and Temkin (C) isotherms at 298 K.

Table 6 Isotherms parameters.

Adsorption isotherm	Parameters	R^2	RMSE	SSE	SD
Langmuir	Q_{max} = 1428.57 mg g^{-1} K_a = 385.57 L mg^{-1}	0.0288	96.85	46,898	39.54
Freundlich	n = 0.954 mg g^{-1} K_f = 3.15 L mg^{-1}	0.9322	1.39	9.67	1.27
Temkin	b = 56.78 K_T = 0.36 (L g^{-1})	0.9607	9.71	471.75	8.87

4. Conclusions

Three conjugated polymers PMPDIA-A, PMPDIA-B and PMPDIA-E were synthesized in acidic, basic aqueous media and enzymatically. Their chemical, optical and electrical properties were determined. PMPDIA-E gave a blue light under PL lamp. The fluorescence quantum yield of PMPDIA-E was calculated to be 9.15% in DMSO solution. PMPDIA-E showed a blue color emission at 350 nm. The E_g' and E_g values of PMPDIA-E, PMPDIA-A and PMPDIA-B were found to be lower than MPDIA. % char values of PMPDIA-E, PMPDIA-A and PMPDIA-B were determined to be 32.77%, 18.76% and 37%, respectively, at 1000 °C. Moreover, the adsorption capabilities of PMPDIA-B was researched to remove methylene blue (MB) from aqueous solution. The kinetic mechanism was investigated by using pseudo-first- and pseudo-second-order kinetic models. For pseudo-second-order R^2 and ARE values were higher than the other kinetic models. So it could conclude that pseudo-second-order model is the suitable model to study the removal of MB on PMPDIA-B. For linear Langmuir Freundlich isotherm SD, SSE, and RMSE were higher than Freundlich isotherm, so it could conclude that Freundlich isotherm model is the suitable isotherm. All results on the adsorption of MB on PMPDIA-B show the applicability of the adsorption study.

Declaration of Competing Interest

The authors declare that they have no known competing financial interests or personal relationships that could have appeared to influence the work reported in this paper.

References

Abbas, R., Hami, H., Waheb, A., Mahdi, N., 2020. Removal of Eriochrom Black T from aqueous solution using Al_2O_3 surface: Linear and non-linear isotherm models, error analysis and thermodynamic studies. Mater. Today:. Proc. 20, 599–604.

Bilici, A., Kaya, İ., Yıldırım, M., Doğan, F., 2010. Enzymatic polymerization of hydroxy-functionalized carbazole monomer. J. Mol. Catal. B Enzym. 64, 89–95.

Blaha, M., Trchova, M., Moravkova, Z., Humpolicek, P., Stejskal, J., 2018. Semiconducting materials from oxidative coupling of phenylenediamines under various acidic conditions. Mater. Chem. Phys. 205, 423–435.

Bulut, Y., Karaer, H., 2015. Adsorption of methylene blue from aqueous solution by crosslinked chitosan/bentonite composite. J. Dispers. Sci. Technol. 36, 61–67.

Çetin, A., Korkmaz, A., Kaya, E., 2018. Synthesis, characterization and optical studies of conjugated Schiff base polymer containing thieno[3,2-b]thiophene and 1,2,4-triazole groups. Opt. Mater. 76, 75–80.

Demir, H.Ö., Kaya, İ., Saçak, M., 2006. Synthesis and characterization of a pyridine-containing Schiff base oligomer. Russ. Chem. Bull. 55, 1852–1855.

Doğan, M., Alkan, M., Demirbaş, Ö., Özdemir, Y., Özmetin, C., 2006. Adsorption kinetics of maxilon blue GRL onto sepiolite from aqueous solutions. Chem. Eng. J. 124, 89–101.

Fajri, L., Nawi, M., Sabar, S., Nawawi, N., 2018. Preparation of immobilized activated carbon-polyvinyl alcohol composite for the adsorptive removal of 2,4-dichlorophenoxyacetic acid. J. Water Process Eng. 25, 269–277.

Fathy, D., Mansour, N., El-Hashash, M., Mazrouaa, A., Mohamed, M., 2020. Impact of environmentally friendly nanoparticles on physical properties of poly(p-phenylenediamine). Egypt. J. Pet. 29, 133–139.

Fungaro, D., Bruno, M., Grosche, L., 2009. Adsorption and kinetic studies of methylene blue on zeolite synthesized from fly ash. Desalin. Water Treat. 2, 231–239.

Gao, M., Zhu, L., Peh, C.K., Ho, G.W., 2019. Solar absorber material and system designs for photothermal water vaporization towards clean water and energy production. Energy Environ. Sci. 12, 841–864.

Ghani, W., Mohd, A., Mahmoud, D., Rebitanim, N., Sanyang, L., Zainudin, R., 2013. Adsorptıon of methylene blue on Sawdust-Derived Biochar and its adsorptıon isotherms. J. Purity, Util. React. Environ. 2, 34–50.

Gupta, R., Sanotra, S., Sheikh, H.N., Kalsotra, B.L., 2013. Room temperature aqueous phase synthesis and characterization of novel nano-sized coordination polymers composed of copper (II), nickel (II), and zinc (II) metal ions with p-phenylenediamine (PPD) as the bridging ligand. J. Nanostruct. Chem. 3, 41.

Han, H., 2008. Synthesis and characterization of montmorillonite/polypyrrole nanocomposite. Polym. Compos. 30, 66–69.

Huang, M., Li, X., Yang, Y., 2001. Oxidative polymerization of o-phenylenediamine and pyrimidylamine. Polym. Degrad. Stab. 71, 31–38.

Huang, Y., Li, J., Chend, X., Wangae, X., 2014. Applications of conjugated polymer based composites in wastewater purification. Roy. Soc. Chem. 4, 62160–62178.

Iqbal, M., Ashiq, M., 2007. Adsorption of dyes from aqueous solutions on activated charcoal. J. Hazard. Mater. B 139, 57–66.

Jawad, A., Abdulhameed, A., 2020. Mesoporous Iraqi red kaolin clay as an efficient adsorbent for methylene blue dye: Adsorption kinetic, isotherm and mechanism study. Surf. Interfaces 18, 1004222.

Jawad, A., Mubarak, N., Abdulhameed, A., 2019. Tunable Schiff's base-cross-linked chitosan composite for the removal of reactive red 120 dye: Adsorption and mechanism study. Int. J. Biol. Macromol. 142, 732–741.

Jiang, J., Zhang, G., Li, L., Zhang, H., Li, N., Wang, Y., He, J., Mao, F., Yu, K., 2020. On-line monitoring of transient radicals and oligomers: o-Phenylenediamine electrooxidation mechanism study by mass spectrometry. Microchem. J. 153, 104390.

Kamacı, M., Kaya, İ., 2016. New low band gap polyurethanes containing azomethine bonding: Photophysical, electrochemical, thermal and morphological properties. J. Taiwan Inst. Chem. Eng. 59, 536–546.

Kant, R., 2012. Adsorption of dye eosin from an aqueous solution on two different samples of activated carbon by static batch method. J. Water Resour Prot. 4, 93–98.

Kaya, İ., Şenol, D., 2014. Synthesis and characterization of aromatic compounds containing imine and amine groups via oxidative polycondensation. Des. Monomers Polym. 17, 557–575.

Kaya, İ., Kolcu, F., 2018. Polymerization of chrysoidine with chemical and enzymatic oxidative preference: Synthesis, characterization, and spectroscopic study. Polym. Adv. Technol. 29, 2515–2528.

Kaya, İ., Çöpür, S., Karaer, H., 2017. Synthesis, characterization and electrochemical properties of poly(phenoxy-imine)s containing carbazole unit. Int J Ind Chem. 8, 329–343.

Kaya, İ., Yağmur, H., 2020. Synthesis and characterization of poly (3,5-diaminobenzoic acid) via enzymatic and oxidative polymerization and application in methylene blue adsorption. J. Mol. Struct. 1216.

Khosravi, A., Vossoughi, M., Shahrokhian, S., 2013. Iran Alemzadeh, HRP-dendron nanoparticles: The efficient biocatalyst for enzymatic polymerization of poly (2,5-dimethoxyaniline). J. Mol. Catal. B Enzym. 90, 139–143.

Kolcu, F., 2019. Characterization and spectroscopic study of enzymatic oligomerization of phenazopyridine hydrochloride. J. Mol. Struct. 1188, 76–85.

Kumbul, A., Göktürk, E., Sahmetlioglu, E., 2016. Synthesis, characterization, thermal stability and electrochemical properties of *ortho*-imine-functionalized oligophenol via enzymatic oxidative polycondensation. J. Polym. Res. 23, 52-.

Li, H., Bai, J., Shi, Z., Yin, J., 2016. Environmental friendly polymers based on Schiff-base reaction with self-healing, remolding and degradable ability. Polymer 85, 106–113.

Mahdavinia, G.R., Massoudi, A., Baghban, A., Shokri, E., 2014. Study of adsorption of cationic dye on magnetic kappa-carrageenan/PVA nanocomposite hydrogels. J. Environ. Chem. Eng. 2, 1578–1587.

Minisy, I., Zasońska, B., Petrovsky, E., Veverka, P., Šeděnková, I., Hromádková, J., Bobera, P., 2020. Poly(p-phenylenediamine)/maghemite composite as highly effective adsorbent for anionic dye removal. React. Funct. Polym. 146, 104436.

Nandi, B., Purkait, G., 2009. Removal of cationic dyes from aqueous solutions by kaolin: Kinetic and equilibrium studies. Appl. Clay Sci. 42, 583–590.

Olmedo-Martínez, J., Vega-Rios, A., Zaragoza-Contreras, E., 2019. Influence of iota-carrageenan on the morphology and electrical properties of poly(ortho-phenylenediamine) based copolymers. Synth. Met. 258, 116192.

Pramodini, S., Poornesh, P., Sudhakar, Y.N., Kumar, M.S., 2013. X(3) and optical power limiting measurements of Polyaniline and its derivative poly(o-toluidine) under CW regime. Opt. Commun. 293, 125–132.

Şenol, D., 2020. Synthesis, structural characterization, enzymatic and oxidative polymerization of 2,6-diaminopyridine. Journal of Fluorescence 30, 157–174.

Şenol, D., Kaya, İ., 2015. Synthesis and characterization of novel polyamines containing different substitute groups via chemical oxidative polymerization. J. Chin. Chem. Soc. 62, 429–438.

Şenol, D., Kaya, İ., 2019. Synthesis and characterization of substituted poly(naphthalene)s with imine bonding containing thiophene unit. Mater. Chem. Phys. 237, 121876.

Sestrem, R., Ferreira, D., Landers, R., Temperini, M., Nascimento, G., 2010. Synthesis and spectroscopic characterization of polymer and oligomers of ortho-phenylenediamine. Eur. Polym. J. 46, 484–493.

Tang, B., Wang, Y., Liang, H., Chen, Z., He, X., Shen, H., 2006. Studies on the oxidation reaction of tyrosine (Tyr) with H_2O_2 catalyzed by horseradish peroxidase (HRP) in alcohol-water medium by spectrofluorimetry and differential spectrophotometry. Spectrochim. Acta, Part A 63, 609–613.

Temizkan, K., Kaya, İ., 2020. Fluorescence quantum yields and chromatic properties of poly(azomethine)s containing pyridine ring. Mater. Sci. Eng., B 252, 114483.

Topal, Y., Tapan, S., Göktürk, E., Şahmetlioğlu, E., 2017. Horseradish peroxidase-catalyzed polymerization of ortho-imino-phenol: Synthesis, characterization, thermal stability and electrochemical properties. J. Saudi Chem. Soc. 21, 731–740.

Tseng, R.L., Wu, F.C., Juang, R.S., 2010. Characteristics and applications of the Lagergren's first-order equation for adsorption kinetics. J. Taiwan Inst. Chem. Eng. 41, 661–669.

Turac, E., Sahmetlioglu, E., 2010. Oxidative polymerization of 4-[(4-phenylazo-phenyimino)-methyl]phenol catalyzed by horse radish peroxidase. Synth. Met. 160, 169–172.

Wen, S., Huang, G., Wu, S., Li, J., Qu, A., 2019. Determinant factors of photocatalytic hydrogen evolution activity for Schiff base conjugated polymers. Chem. Eng. J. 374, 1055–1063.

Yapa, M., Mubarak, N., Sahu, J., Abdullah, E., 2017. Microwave induced synthesis of magnetic biochar from agricultural biomass for removal of lead and cadmium from wastewater. J. Ind. Eng. Chem. 45, 287–295.

Yuvaraja, G., Chen, D., Pathak, J., Long, J., Subbaiah, M., Wen, J., Pan, C., 2020. Preparation of novel aminated chitosan Schiff's base derivative for the removal of methyl orange dye from aqueous environment and its biological applications. Int. J. Biol. Macromol. 146, 1100–1110.

Zoromba, M., Al-Hossainy, A.F., 2020. Doped poly(o-phenylenediamine-co-p-toluidine) fibers for polymer solar cells applications. Sol. Energy 195, 194–209.